

# The Effectiveness of Magnetic Shielding in High- $I_{sp}$ Hall Thrusters

Ioannis G. Mikellides,<sup>\*</sup> Richard R. Hofer,<sup>†</sup> Ira Katz<sup>‡</sup> and Dan M. Goebel<sup>§</sup>  
*Jet Propulsion Laboratory, California Institute of Technology, Pasadena, CA, 91109*

**Abstract:** A series of numerical simulations and experiments have been performed to assess the effectiveness of magnetic shielding in a Hall thruster operating in the discharge voltage range of 300-700 V ( $I_{sp} \approx 2000-2700$  s) at 6 kW, and 800 V ( $I_{sp} \approx 3000$ ) at 9 kW. In this paper we report on the simulation results and their validation with experimental measurements. At 6 kW the magnetic field topology with which we recently demonstrated highly effective magnetic shielding at 300 V was retained for all other discharge voltages; only the magnitude of the field was changed to achieve optimum thruster performance. It is found that magnetic shielding remains highly effective for all discharge voltages studied. Maximum erosion rates that remain fairly constant across the range of 300-700 V are computed, with values not exceeding  $10^{-2}$  mm/kh. Such rates are  $\sim 3$  orders of magnitude less than those observed in the unshielded version of the same thruster at 300 V. At 9 kW and 800 V, saturation of the magnetic circuit did not permit us to attain precisely the same magnetic shielding topology as that employed during the 6-kW operation since this thruster was not designed to operate at this condition. Consequently, the maximum erosion rate at the inner wall is found to be  $\sim 1$  order of magnitude higher ( $\sim 10^{-1}$  mm/kh) than that at the 6-kW level. At the outer wall the ion energy is below the sputtering yield threshold so no measurable erosion is expected. The reasons behind the effectiveness of magnetic shielding at higher discharge voltages are discussed.

Since their inception over several decades ago the application of Hall thrusters has been limited to near-Earth missions largely due to their limited throughput capability. The source of this limitation has been erosion of the acceleration channel walls, which can lead to exposure of critical magnetic circuit components to the high-energy ion beam and, eventually, to engine failure. Recently a new technique was demonstrated to eliminate channel erosion in Hall thrusters [1] based on findings from physics-based numerical simulations with a magnetic-field-aligned-mesh (MFAM) code called *Hall2De*. [2] Termed “magnetic shielding,” the technique enforces the equipotentialization of specific magnetic field lines termed “grazing lines” which, in turn, protect the channel walls from ion bombardment. Deviations from equipotentialization along lines of force in Hall thrusters occur naturally in the bulk of the acceleration channel due to the finite electron temperature ( $T_e$ ) and the variation of the electron number density ( $n_e$ ) along these lines. In thrusters with unshielded (US) walls these deviations allow for a component of the induced electric field ( $\mathbf{E}$ ) along the magnetic field ( $\mathbf{B}$ ) that is significantly large to accelerate some beam ions towards the walls causing erosion.

Magnetic shielding was enabled by two major events: (1) Aerojet designed and built the BPT-4000 that demonstrated a zero-erosion state after 5,600 h of qualification testing [3], and (2) the Jet Propulsion Laboratory (JPL) performed numerical simulations that explained the physics behind these test results. [4]. The simulations also explained why erosion of this thruster in the beginning of the life test occurred at rates observed in other Hall thrusters, and why it stopped after material was eroded away to expose a critical magnetic field topology to the plasma. These explanations led to the development of the theory

---

<sup>\*</sup> Principal Engineer, Electric Propulsion Group, 4800 Oak Grove Drive, Pasadena, CA, 91109, Mail Stop 125-109, Associate Fellow AIAA.

<sup>†</sup> Senior Engineer, Electric Propulsion Group, 4800 Oak Grove Drive, Pasadena, CA, 91109, Mail Stop 125-109, Associate Fellow AIAA.

<sup>‡</sup> Group Supervisor, Electric Propulsion Group, 4800 Oak Grove Drive, Pasadena, CA, 91109, Mail Stop 125-109, Senior Member AIAA.

<sup>§</sup> Senior Research Scientist, Thermal and Propulsion Engineering Section, 4800 Oak Grove Drive, Pasadena, CA, 91109, Mail Stop 125-109, Fellow AIAA.

behind magnetic shielding, followed by a laboratory demonstration of a magnetically shielded (MS) Hall thruster called the H6MS [5-7]. During this 2-yr, proof-of-principle effort, development of a new thruster was unfeasible so our approach was to modify the channel geometry and magnetic field of an existing thruster - a 6-kW laboratory Hall thruster called H6 [8] - with the guidance of physics-based numerical simulation. Hereinafter we shall term the unshielded version of this thruster the H6US. The demonstration of the H6MS was performed at a discharge voltage ( $V_d$ ) of 300 V and discharge current ( $I_d$ ) of 20 A.

Magnetic shielding relies heavily on our ability to achieve low  $T_e$  along the grazing lines of force. A natural question then arises about the effectiveness of this technique to protect the channel walls in thrusters operating at  $V_d > 300$  V, where electrons are expected to be hotter. Maximum values of  $T_e$  in these thrusters vary typically between 10-20% of the discharge voltage. The question is of immediate significance to ongoing thruster development and testing activities at the NASA Glenn Research Center (GRC) and JPL aimed at supporting NASA's Asteroid Initiative, which includes a proposal to robotically capture a small near-Earth asteroid and redirect it safely to a stable orbit in the Earth-moon system where astronauts can visit and explore it (Fig. 1).[9] Trajectory studies have shown that an Asteroid Redirect Mission (ARM) will require Hall thrusters operating at a specific impulse ( $I_{sp}$ ) of  $\sim 3000$  s.[10, 11] Moreover, these thrusters will be expected to deliver a throughput of 12,000 kg of xenon [11], which is nearly a factor 30 greater than the 425 kg launched on the Dawn mission (the largest xenon propellant load launched to date). In response, NASA's Space Technology Mission Directorate, In Space Propulsion Project is supporting investigations of magnetic shielding in high- $I_{sp}$  thrusters. These investigations include numerical simulations, thruster modifications and testing of the NASA 300M, a 20-kW Hall thruster developed at GRC [REF], and of the H6MS Hall thruster developed at JPL [5-7]. The main objective of the most recent work with the H6MS at JPL has been to demonstrate magnetic shielding at high discharge voltages culminating with a wear test at 9 kW and 800 V.



*Fig. 1 The Asteroid Redirect Mission (ARM) proposes to capture robotically a small near-Earth asteroid and redirect it safely to a stable orbit in the Earth-moon system. ARM will require long-life Hall thrusters that can deliver 3000 sec of  $I_{sp}$  (input voltage to each thruster of  $\sim 800$  V).*

In this paper we report on the results from numerical simulations of the H6 thruster intended to assess the effectiveness of magnetic shielding in the range of 300-800 V. For brevity we shall follow the naming convention (*Discharge power*)(*MS or US*)(*Discharge voltage*) when referring to the thruster configuration and its operating condition. For example, the unshielded thruster operating at 6 kW and 300 V will be referred to as the 6US300 condition or configuration, the magnetically shielded thruster at 9 kW and 800 V will be called 9MS800 and so on and so forth. Section I provides a summary of the first principles of magnetic shielding and describes briefly the models and methods used in the numerical simulations. Section II reports simulation results for the H6MS in the range of 300-700 V and compares these results with plasma measurements obtained in the Owens vacuum facility at JPL. Section III reports simulation results for the H6MS at 9 kW and 800 V and compares these results with a limited set of data from the  $\sim 115$ -h wear test. A detailed report of the performance and wear test data is planned for another publication in the near future. The paper concludes with Sec. IV.

## I. Theory and Models

### A. Magnetic Shielding First Principles

The theory behind magnetic shielding was discussed in detail in previous publications.[1, 6, 7] In this section we provide only a summary of the main points for completeness. We begin with a brief review of well-known operational characteristics of Hall discharges as they are critical in establishing some of the

key elements that allow magnetic shielding to be effective. The number density of electrons in Hall thrusters is low enough such that collisions in the azimuthal direction seldom impede their  $\mathbf{E} \times \mathbf{B}$  drift, yielding in this direction a significant flow of current, the Hall current. Operation under these conditions implies a high value of the Hall parameter for the electrons,  $\Omega_e \equiv \omega_{ce}/\nu_e \gg 1$ , where  $\omega_{ce}$  and  $\nu_e$  are the electron cyclotron and total collision frequencies, respectively. As the Hall current crosses  $\mathbf{B}$  the induced  $\mathbf{E}$  is in the direction perpendicular ( $\perp$ ) to  $\mathbf{B}$  and proportional to  $\sim \eta \Omega_e^2 \mathbf{j}_{e\perp}$  (according to Ohm's law).  $\mathbf{E}_\perp/q_i$  serves as the main acceleration force on the ions. Here, the electron current density and resistivity are denoted by  $\mathbf{j}_e$  and  $\eta$ , respectively. The increased resistive heating of the electrons in the region of high  $\mathbf{E}$  leads also to an increase in  $T_e$ . Typical profiles of the plasma potential ( $\phi$ ) and  $T_e$  along the channel centerline (CL) are shown in the schematic of Fig. 2-left.

Under typical discharge conditions in Hall thrusters the resistance to the transport of heat and mass in the electron flow in a direction parallel ( $\parallel$ ) to  $\mathbf{B}$  is much smaller (by  $\sim \Omega_e^2$ ) than that in the  $\perp$  direction for most of the channel region. Thus,  $T_e$  remains relatively unchanged along the lines of force:

$$\nabla_{\parallel} T_e \approx 0 \quad (1)$$

Moreover, in the absence of a resistive contribution to  $\mathbf{E}$  in this direction the electron momentum equation simplifies to:

$$\mathbf{E}_{\parallel} \approx -T_e \nabla_{\parallel} \ln(n_e) \quad (2)$$

Equations (1) and (2) yield respectively two well-known properties of the lines of force in these thrusters[12, 13]:  $T_e \approx T_{e0}$  and  $\phi \approx \phi_0 + T_{e0} \ln(n_e/n_{e0})$  along a magnetic field line, where  $T_{e0}$ ,  $\phi_0$  and  $n_{e0}$  denote integration constants. Thus, though each line is nearly isothermal it is not also of fixed potential unless the electron temperature is zero. This allows for a finite component of  $\mathbf{E}$  parallel to  $\mathbf{B}$  which, in turn, can lead to ion acceleration towards the containing walls if the  $\mathbf{B}$ -lines begin/terminate at the surface of the material. Erosion of the channel walls occurs when ions strike them with sufficient energy to sputter off material.

Deviations from equipotentiality along lines of force near the channel walls has been the main reason that most state-of-the-art (SOA) Hall thruster designs have continued to experience channel erosion. To better illustrate the main impediment we use as an example a typical SPT-like magnetic field configuration as depicted in Fig. 2-middle. We designate this as a ‘‘US configuration.’’ Here the variation of  $\phi$  and  $T_e$  along the walls is similar to that along the CL because the lines are nearly radial. Consequently, the elevated  $E_{\parallel}$  and  $T_e$  at the walls can drive a flux of high-energy ions to the walls. The induced erosion can be reduced marginally if the curvature of lines is made more convex towards the anode as originally proposed by Morozov *et al.*[13] By comparison, magnetic shielding reduces erosion rates by orders of magnitude in the beginning-of-life configuration of the thruster.

Referring to Fig. 2-right, magnetic shielding is achieved by way of a magnetic field topology that sustains high  $\phi$  and low  $T_e$  along the channel-grazing magnetic field lines, in fact, as close as possible to the discharge voltage  $V_d$  and to the coldest values of  $T_e$  that can be attained inside the channel, respectively. In this manner the incident-ion kinetic and sheath energies can be marginalized. Moreover, with a properly designed combination of  $\mathbf{B}$  and channel geometry,  $\mathbf{E}$  can be controlled to be both nearly perpendicular to the surface and large in magnitude, as shown in the MS configuration Fig. 2-right. In this manner the induced  $\mathbf{E}_{\perp}$  forces ion acceleration away from walls without loss of thruster performance. This also reduces the wall-incident ion flux. It is emphasized that a change in the geometry of the wall alone, e.g. chamfering of the surface, is not sufficient as it has been demonstrated in our previous tests.[6] The key principle behind magnetic shielding lies in the recognition that the electron pressure (yielding  $T_e \times \ln(n_e)$  in Eq. (1)) forces  $\mathbf{E}$  and  $\mathbf{B}$  to no longer form an orthogonal set (Fig. 2-middle). Thus, a geometry of  $\mathbf{B}$ -lines with convex curvature toward the anode cannot effectively control  $\mathbf{E}$  near surfaces (and, in

turn, the erosion) if the near-wall lines are not also equipotential. In contrast, Fig. 2-right shows a magnetically shielding  $\mathbf{B}$  topology. This topology eliminates the contribution of the electron pressure by exploiting those  $\mathbf{B}$ -lines that extend deep inside the acceleration channel, near the anode. Because these lines are associated with high  $\phi_0$  and low  $T_{e0}$  the contribution of  $T_e \times \ln(n_e)$  is marginalized. The question this paper aims to answer is whether magnetic shielding remains effective at higher discharge voltages where both  $T_e$  and  $\phi$  are higher as well. We argue that if magnetic shielding is to remain effective under these conditions the critical ability to demonstrate is the sustainment of low  $T_e$  near the anode as this would ensure the constancy of the plasma potential along the grazing lines. If this was achieved then, in principle, the magnitude of this plasma potential would be of little significance to erosion and magnetic shielding would remain effective at higher discharge voltages.

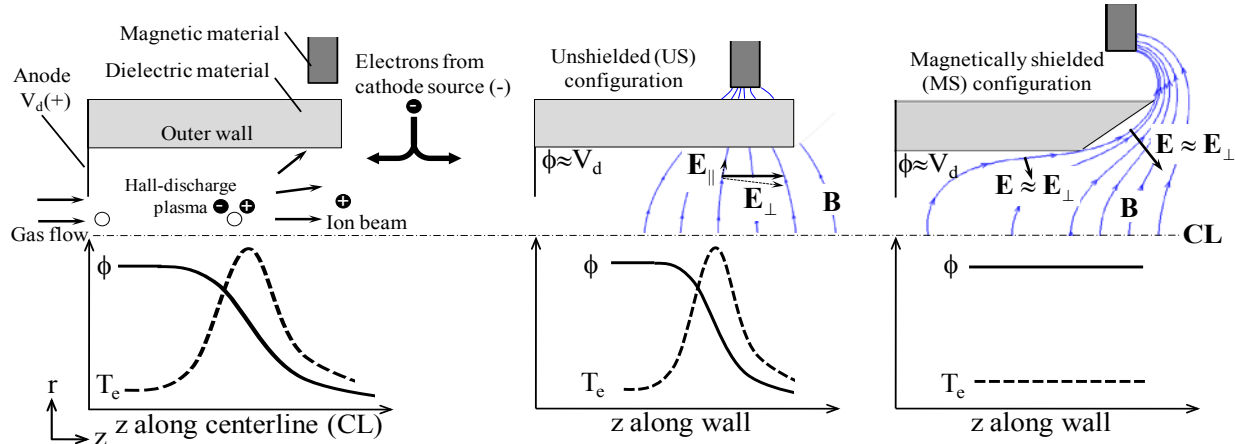


Fig. 2. Schematics of the upper half of the annular acceleration channel in a typical magnetic-layer Hall thruster (top) and typical profiles of  $\phi$  and  $T_e$  (bottom) established during ion acceleration. Left: Basic features of the accelerator and typical profiles along the CL. Middle: Representative magnetic field lines and profiles along the wall in a US configuration. Right: Representative magnetic field lines and profiles along the wall in a MS configuration. The line that extends deepest into acceleration channel and runs closest to the channel wall without crossing it is termed the “grazing line.”

## B. Numerical Simulations

### 1. Methods

The numerical simulations have been performed with the Hall2De code, [2, 14] a two-dimensional (2-D) computational solver of the conservation equations that govern the evolution of the partially ionized gas in Hall thrusters. The governing equations, numerical methodology, various thruster simulations and comparisons with measurements have been presented elsewhere.[2, 5, 7] Here, we provide only a brief overview of the code for completeness.

Excessive numerical diffusion due to the large disparity of the transport coefficients parallel and perpendicular to the magnetic field is evaded in Hall2De by discretizing the equations on a computational mesh that is aligned with the applied magnetic field. The MFAM capability in Hall2De was largely motivated by the need to assess the life of Hall thrusters with complicated magnetic field topologies. Shown in Fig. 3-left is a schematic of the computational domain used in the H6 simulations with naming conventions of various thruster components and boundaries. A photograph of the thruster operating in a vacuum facility at JPL is shown in Fig. 3-right. The MFAM spans a computational domain in  $r$ - $z$  geometry that extends several times the thruster channel length in the axial direction, and encompasses the cathode boundary and the thruster CL. The numerical solution of the conservation equations for the heavy species is obtained without invoking discrete-particle methods. The evolution of the (collisionless) neutral species is computed using line-of-sight formulations that account for ionization.[14] Ions are treated as an isothermal, cold (relative to the electrons) fluid, accounting for the drag force and the ion-pressure gradient. Up to triply-charged ions and up to four distinct ion fluids can be included in Hall2De.

In the H6 simulations presented here three charge states were accounted for but all ions were considered to be part of a single fluid. The electron population in Hall2De is treated also as a fluid. The solution of the electron energy conservation equation provides  $T_e$ . Ohm's law is solved in the frame of reference of the magnetic field with the electrical resistivity accounting for contributions from collisions of electrons with all other species. It has also been argued that the diffusion of electrons in Hall thrusters is enhanced in a non-classical manner by plasma turbulence [15-18]. In numerical simulations this enhancement has typically been modeled using an effective or "non-classical" collision frequency. Denoting this collision frequency as  $\nu_\alpha$ , we impose in Hall2De a so-called transport coefficient function  $f_\alpha(r,z)$  and set

$$\nu_\alpha = f_\alpha \omega_{ce}. \quad (3)$$

Our specification of  $f_\alpha$  is guided by plasma measurements whenever they exist. In the present simulations plasma measurements that spanned both the interior of the acceleration channel and the plume region existed only at the 300-V case. Thus,  $f_\alpha$  at  $V_d > 300$  V was implemented by assuming that its general spatial variation did not vary but its magnitude was determined by iterations guided by the measured  $I_d$  and thrust (F).

The conservation equations for the electrons are closed with boundary conditions (BC) at all surfaces shown in Fig. 3-left. The channel (ring) walls and the thruster front plate are dielectric boundaries. At the anode we impose sheath BCs for the electron current density normal to the anode. At the cathode boundary the neutral particle flux, ion flux, plasma potential and electron temperature are specified. For all dielectric-wall boundaries a zero-current condition is imposed. At these surfaces the BC for the convective heat loss follows the formulations of Hobbs and Wesson [19] for the potential drop in a sheath with secondary electron emission. The far plume solution is subject to outflow BCs. The energy equation is solved in a semi-implicit fashion; the thermal conduction term is implicit whereas all other terms are evaluated explicitly. Current conservation, incorporating Ohm's law to solve for the electron current density, is also solved implicitly.

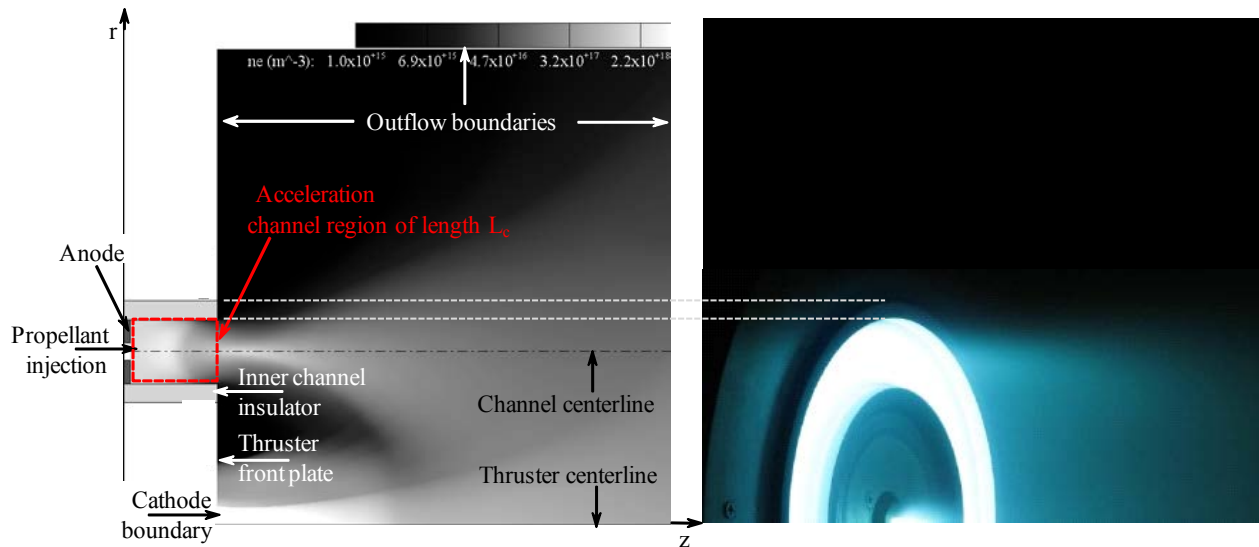


Fig. 3. Left: Computational domain of the H6 laboratory Hall thruster showing naming conventions for the various thruster components and boundaries that are cited throughout this paper. Right: Photograph of the thruster operating in a vacuum facility at JPL.

## 2. Erosion Model

Channel erosion in Hall2De accounts for contributions from  $\text{Xe}^+$ ,  $\text{Xe}^{++}$  and  $\text{Xe}^{+++}$ . The sputtering erosion rate ( $\varepsilon$ ) due to ion bombardment is given by,

$$\varepsilon = j_{i\perp} Y \quad (4)$$

where the incident ion current density perpendicular to the channel wall,  $j_{i\perp}$ , is dependent on the ion number density ( $n_i$ ) and the ion velocity ( $u_i$ ) at the wall. The sputtering yield of the channel material,  $Y$  (expressed throughout the paper in  $\text{mm}^3/\text{C}$ ) is a function of the ion impact energy ( $K$ ) and incidence angle ( $\beta$ ). Because ions must traverse a sheath before striking the wall, the total impact energy is the sum of the kinetic energy  $K_i = \frac{1}{2} m_i u_i^2 / q_i$  (expressed in units  $\text{J}/\text{C}$ ) ions of mass  $m_i$  have acquired in the plasma upon entrance to the sheath, and the sheath potential energy denoted as  $\Delta\phi$ . That is,

$$j_{i\perp} = j_{i\perp}(q_i, n_i, u_{i\perp}) \quad Y = Y(K_i + \Delta\phi, \beta) \quad (5)$$

The potential energy  $\Delta\phi$ , transformed to ion kinetic energy as the plasma ions are accelerated inside the sheath towards the solid material, is computed based on the solution to the 1-D sheath equations in the presence of secondary electron emission. Hobbs and Wesson showed that the sheath equations for this problem consist of a system of three non-linear equations for the electric field, sheath potential and ion Mach number. For ease of computation in the numerical simulations we employ a fit [20]  $\Delta\phi = \Delta\phi(T_e)$  to the solution of these equations. In the numerical simulations the vertex-centered  $\mathbf{u}_i$  and the element-centered  $n_i$  at each computational element adjacent to the wall boundary are used to determine the total impact energy  $K = K_i + \Delta\phi$  and angle  $\beta$ . Then the sputtering yield is determined as follows:

$$Y = f_\beta(\beta) f_K(K). \quad (6)$$

The fitting functions we have used are  $f_K(K_i + \Delta\phi)$  for the energy dependence at zero angle of incidence and  $f_\beta(\beta)$  for the angle dependence:

$$f_\beta(\beta) = \cos(\beta)^{-c_0} \exp[-c_1(\cos(\beta)^{-c_2} - 1)] \quad f_K(K) = \begin{cases} c_3 \left[ 1 - \left( \frac{K_T}{K} \right)^{2/3} \right] \left( 1 - \frac{K_T}{K} \right)^2 & K \geq K_T \\ 0 & K < K_T, \end{cases} \quad (7)$$

and are plotted in Fig. 4. For the boron-nitride (BN) material used in the thruster studied here there are only limited measurements of the sputtering yield, most of which provide values for energies  $\geq 100$  V. [21-23] Recently, measurements at energies  $< 100$  V were produced by Rubin *et al.* [23] However, Rubin *et al.* also acknowledged that their values were higher than published data. While they discussed possible sources of this discrepancy, investigations to confirm its/their identity had not yet been completed. Hence, in our simulations we have relied on the work of Garner *et al.* [21] and of Yalin *et al.* [22] to guide  $f_K$ . Their data are plotted in Fig. 4-right. Regarding the choice of  $K_T$  in Eq. (7)-right, based on a series of sensitivity simulations and comparisons with profilometry measurements in the H6US thruster we have found that  $25 \lesssim K_T \lesssim 50$  V covers the range within which the true  $K_T$  most likely resides for BN. [6, 7] This is also in agreement with the conclusions of Shastry.[24] Because a single value of  $K_T$  remains unknown, in the present work we consider both limits. To illustrate the differences in the sputtering yield, two functions  $f1_K$  and  $f2_K$  are plotted in Fig. 4-right corresponding to  $K_T = 25$  V and 50 V, respectively. In the Hall2De code  $\varepsilon$  is set to zero when  $K < K_T$ .

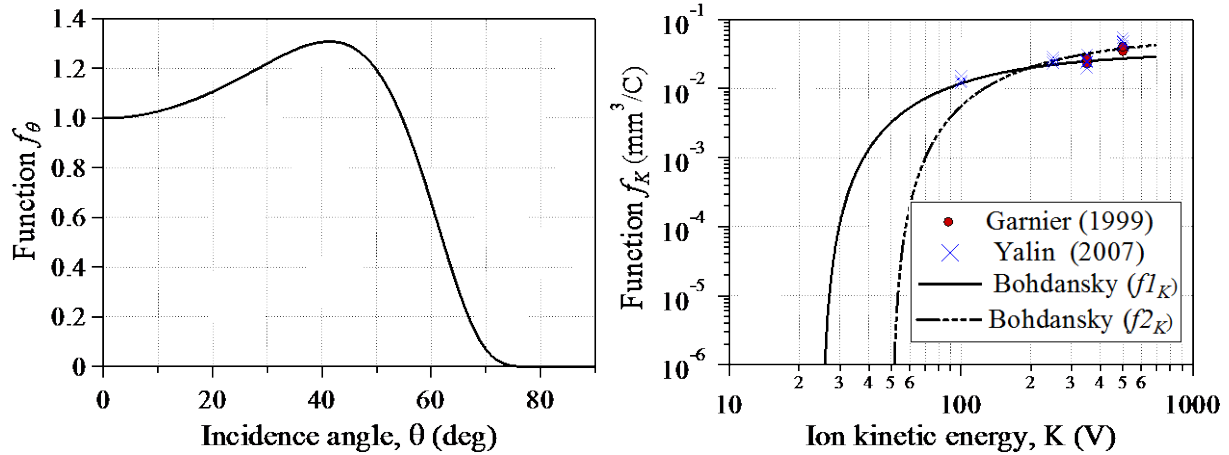


Fig. 4. Fitting functions for the sputtering yield of the BN channel material used in the Hall thruster simulations. Left: The coefficients for the angle dependence function  $f_\theta$  (Eq. (7)-left) are  $c_0=7.19$ ,  $c_1=5.4$ ,  $c_2=1$ . Right: Energy dependence function  $f_K$  (Eq. (7)-right) for two choices of the sputtering yield threshold. The coefficients are  $c_3=0.035$ ,  $K_T=25$  for  $f1_K$ , and  $c_3=0.06$ ,  $K_T=50$  for  $f2_K$ .

## II. Simulation Results and Comparisons with Experiments at the 6-kW Power Level

### A. Plasma and thruster performance

We present in this section results from Hall2De simulations of the H6MS in the discharge voltage range of 300-700 V. All results in this range have been at the operating power of 6 kW. An additional simulation at 9 kW and 800 V has been performed the results of which are presented in the next section. Operation at  $I_d=20$  A and  $V_d=300$  V will be referred to as the nominal operating condition.

Though only negligible differences were observed between the measured and modeled magnetic shielding field topologies at the 6MS300 operation, all simulations presented here have used the measured magnetic field. The measurements were obtained using a 3-axis gaussmeter [6]. Also, a higher-resolution computational grid was constructed and used for all simulations in the range 300-700 V compared to that used in our 2012 simulations at the 6MS300 condition[1, 7]. We found negligible differences in the results between the two grid arrangements. The magnetic shielding field topology was held fixed in all simulations at the 6-kW power level compared to that at the nominal condition, but its magnitude was scaled linearly with the inner coil current values specified in the experiments. The radial components of the magnetic field along the channel centerline as implemented in the H6MS 300-700 V simulations are plotted in Fig. 5. All thruster operating conditions required for the Hall2De simulations - the anode and cathode flow rates, the discharge voltage and the background pressure - were provided by the experiments.

Far plume plasma measurements at 300 V were used to assign values of  $T_e$  at the outflow boundaries, while internal and near-plume plasma and performance measurements for the discharge current and thrust were used to guide the specification of the collision frequency,  $\nu_\alpha$ . In previous work [5, 7] we found that  $f_\alpha$  exhibited significant deviations from a constant and argued that there was no strong evidence to support a Bohm-like dependence (i.e.  $\propto \omega_{ce} \propto |B|$ ) of  $\nu_\alpha$ . More recently, a detailed investigation of the effects of the collision frequency  $\nu_\alpha$  was undertaken, the results of which are beyond the scope of this paper and are therefore reserved for a future publication. This recent work has led to a better understanding of the spatial variation of  $\nu_\alpha$  both inside and outside the acceleration channel of this thruster and, as such, the simulations now predict the behavior of the thruster more accurately compared to our previous simulations at 300 V.[7] Table 1 shows that for both the US and MS thruster configurations the discrepancy between experiment and simulation for all performance related quantities compared is less than 5.6%, with the exception of the singly- and triply-charged ion fractions. In light of the limited data that exist for the ionization cross sections of these species we speculate without proof that these higher

discrepancies may be due to errors in these cross sections. Regarding any correlations with Bohm-like variation of  $v_\alpha$  at the higher discharge voltages, we find (as in the 300-V cases) that the frequency is not proportional to  $|B|$  in the vicinity of the acceleration region, as suggested by the comparison in Fig. 5 (we note that  $B_z \ll B_r$  along the channel CL). The total classical collision frequency is found to be less significant compared to  $v_\alpha$  inside the channel with increasing discharge voltage.

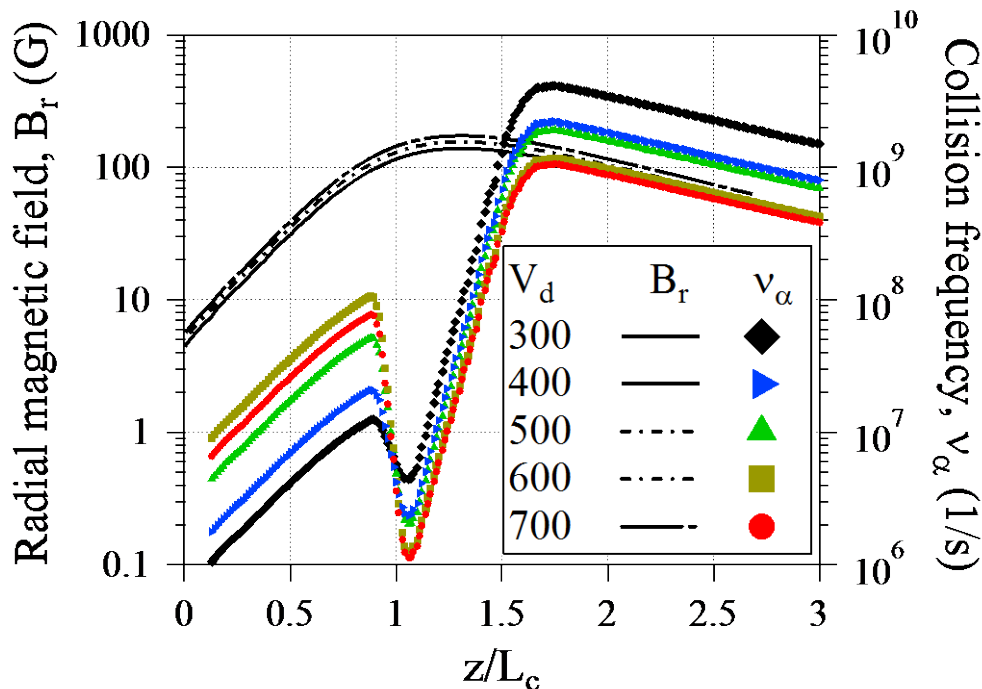


Fig. 5. Channel centerline profiles of the radial component of the magnetic field as implemented in both the thruster experiments and numerical simulations. Also plotted is the collision frequency  $v_\alpha$  implemented in the numerical simulations. The simulations suggest significant deviations of  $v_\alpha$  from  $\sim B$  (i.e. Bohm-like) dependence in the vicinity of the acceleration region for all discharge voltages examined.

Table 1. Comparisons of thruster performance parameters in the H6US and H6MS configurations at the operating condition of 300 V and 6 kW.

Performance parameter	6US300			6MS300		
	Exp.	Sim.	%Disc.	Exp.	Sim.	%Disc.
Discharge voltage, $V_d$ (V)	300	300	0	300	300	0.0
Discharge current, $I_d$ (A)	20	20	0	20.02	20.02	0.0
Anode flow rate (mg/s)	19.7	19.7	0	18.35	18.35	0.0
Cathode flow rate (mg/s)	1.37	1.38	-0.7	1.28	1.28	0.0
Ion beam current (A)	16.7	16.18	3.1	17.4	17.1	1.7
Thrust, F (mN)	401.0	400	0.2	387.2	387.7	-0.1
Xe <sup>+</sup> current fraction	0.755	0.720	4.6	0.575	0.570	0.9
Xe <sup>++</sup> current fraction	0.161	0.260	-61.5	0.259	0.377	-45.6
Xe <sup>+++</sup> current fraction	0.064	0.020	68.8	0.119	0.053	55.5
Xe <sup>++++</sup> current fraction	0.02	N/A*	N/A*	0.047	N/A*	N/A*
Current utilization	0.835	0.809	3.1	0.870	0.854	1.8
Mass utilization	0.931	0.964	-3.5	0.931	0.983	-5.6

\*Hall2De simulations only accounted for up to triply-charged Xe ions.

The simulation results for  $T_e$  and  $\phi$  along the channel centerline at the 6MS300 condition from the new simulations are plotted in Fig. 6. Compared to our previous (2012) results [7] we achieve here better accuracy based on the comparisons with the plasma measurements. Specifically, it is found that the overestimation of the computed electron temperature in the near plume region that was observed during our previous simulations was reduced only by modifications of  $v_\alpha$  inside the channel. Despite such improvements however, the simulation continues to overestimate in general the measured  $T_e$  which suggests that some energy loss mechanism(s) is(are) either not accounted for or not well understood. The maximum  $T_e$  is found to be  $\sim 30\%$  less in the simulations than the experiments. Though no such measurements exist yet for  $V_d > 300$  V, similar discrepancies are expected at the higher discharge voltages as well. Regarding effects on erosion, overestimates in  $T_e$  imply also higher erosion rates due to the increased energies that ions could gain through the sheath, so our simulation results would in fact be conservative in this regard. The good agreement obtained between experiments and simulations for the plasma potential as well for the performance of the thruster at 300 V, allowed the 6MS300 simulation to serve as the basis for the remaining simulations at the higher discharge voltages for which only limited plasma measurements were available for comparisons. The comparisons are shown in Fig. 6-right and summarized in Table 2. Similarly to the 300-V cases, we find the discrepancies between experiment and simulation to be small, approximately less than 3%. Regarding thruster performance, the total efficiency of the thruster was measured to be between 61.2-63.7% in the range of 300-700 V. Compared to the 6US300 operation, the efficiency decreased at the 6MS300 from 63.5% to 62.7%. A more detailed account of all the measurements performed in this range of operating conditions will be reported in a future publication.

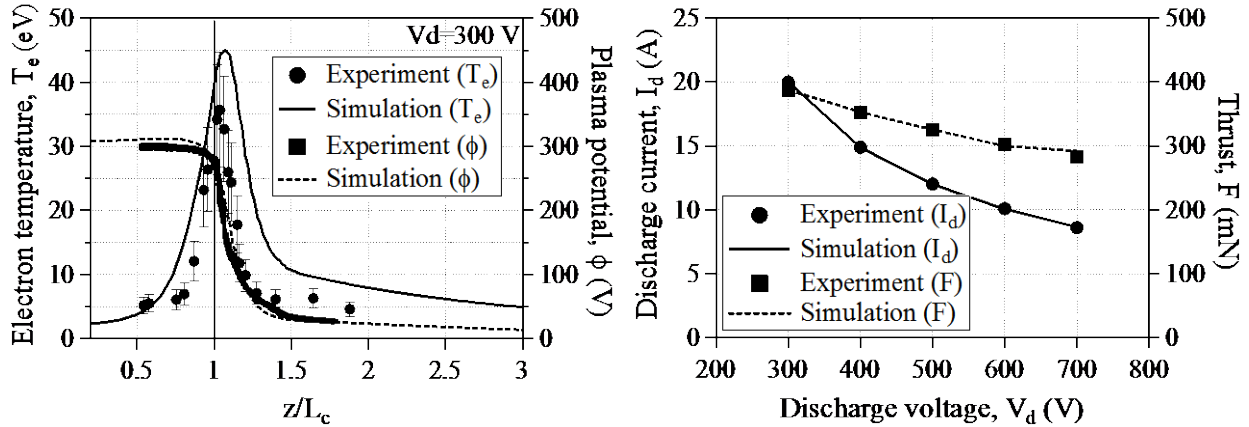


Fig. 6 Left: Comparison between simulations and measurements of  $\phi$  and  $T_e$  along the channel centerline in the H6MS at 6 kW, 300 V. Right: Comparison between numerical simulation results and measurements of the discharge current and thrust of the H6MS at various discharge voltages.

Table 2. Comparison between simulations and experiments in the discharge voltage range 300-700 V of the H6MS. The discrepancy is provided as  $\%(\text{Experiment-Simulation})/\text{Experiment}$ . The background pressure varied between  $1 \times 10^{-5} - 1.7 \times 10^{-5}$  Torr during the tests and was specified in the simulations directly from measurements for each operating discharge voltage.

$V_d$ (V)	Experiment			Simulation			% Discrepancy		
	$I_d$ (A)	$F$ (mN)	$I_{sp}$ (s)	$I_d$ (A)	$F$ (mN)	$I_{sp}$ (s)	$I_d$ (A)	$F$ (mN)	$I_{sp}$ (s)
300	20.02	387.2	1997	20.02	387.7	1998	0.0	-0.1	-0.1
400	14.88	352.8	2225	14.88	353.1	2244	0.0	-0.1	-0.9
500	12.0	325.3	2385	11.99	325.4	2386	0.1	0.0	0.0
600	10.12	302.7	2539	10.05	299.9	2486	0.7	0.9	2.1
700	8.6	283.3	2683	8.65	292.0	2756	-0.6	-3.1	-2.7

The simulation results on the variation of  $T_e$  and  $\phi$  along the channel centerline are compared in Fig. 7 for the range of 400-700 V. The 300-V result from Fig. 6 is also included for completeness. We find that although the maximum electric field, and therefore the majority of the acceleration, occur downstream of the channel exit (i.e for  $z/L_c > 1$ ), for all discharge voltages, this acceleration begins deeper into the channel the lower the discharge voltage. This can be seen in Fig. 7-left where the plasma potential exhibits the most gradual variation with  $z/L_c$  near the exit plane at 300 V, becoming steeper as  $V_d$  increases. Also evident in Fig. 8, which plots contours of  $n_e$  overlaid by vectors of the singly-charged ion flux, is a purely two-dimensional effect associated with the structure of the ion flux vector field at the chamfered regions of the channel. Ions appear to become slightly more divergent near the channel exit which implies more of them can strike the chamfered walls. However, if magnetic shielding is effective in sustaining near-constant  $\phi$  and low  $T_e$  along these walls (per Fig. 2-right), thereby reducing the energy of these ions, such increase in the ion flux should have only a small effect on erosion. This is because in magnetically shielded thrusters, where the ion velocity to the walls is reduced significantly (compared to unshielded thrusters), the erosion rate is much more sensitive to changes in the ion energy (see Fig. 4-right) whereas its dependence on the ion flux is only linear. The expected rise of the maximum  $T_e$  with discharge voltage is also obtained and found to range 15-18% of the discharge voltage as shown in Fig. 8-right and Fig. 8 middle and bottom. Regarding implications on erosion, it is emphasized that the higher electron temperatures that are obtained as the discharge voltage increases will yield higher erosion rates only if the magnetic shielding topology is not effective in keeping electrons cold near the channel walls. This is discussed further in the next section.

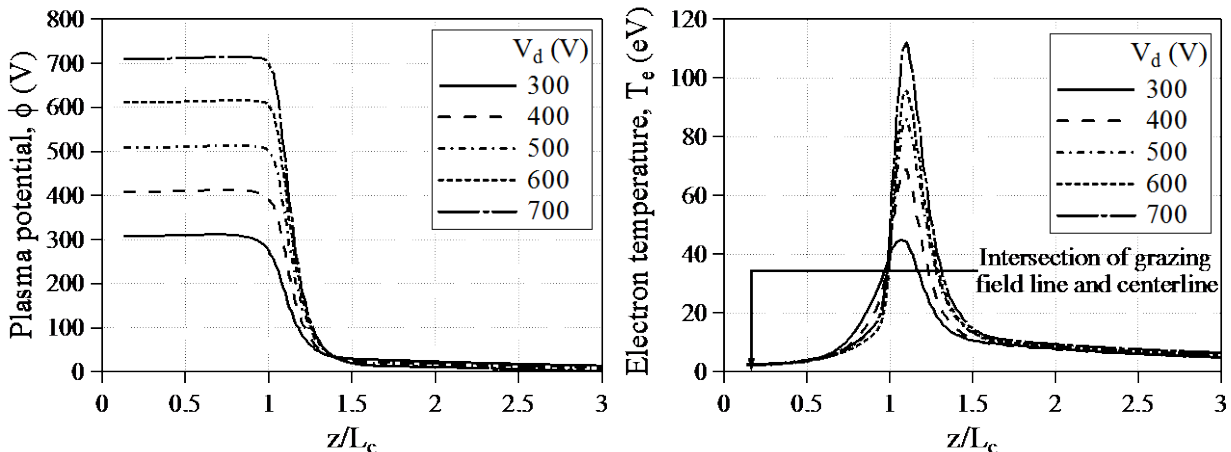


Fig. 7. Computed plasma potential (left) and electron temperature (right) along the channel centerline of the H6MS in the discharge voltage range of 300-700 V.

## B. Erosion of the channel walls

The computed plasma properties from the simulations have been used in the erosion model described in Sec. I.B.2 to assess the effectiveness of magnetic shielding in the range of 300-700 V. We find that the desired behavior of the plasma along the channel walls, as described in Sec. I.A is achieved at all discharge voltages. Specifically, Fig. 9-left shows that the plasma potential for all cases along the inner wall is sustained at a near-fixed value that is close to the discharge voltage. The same behavior is found at the outer wall. This is largely driven by the low electron temperatures achieved near this region as shown in Fig. 9-right. Two noteworthy findings here is that the computed  $T_e$  along the chamfered walls does not exceed  $\sim 2.5$  eV, and that its value studied does not vary significantly with discharge voltage. Because the grazing magnetic field line at the inner wall extends deep into the anode region in this thruster, the low  $T_e$  values observed along the near-exit portions of channel walls is nothing but a reflection of the low  $T_e$  values that persist near the anode. This can easily be seen in Fig. 7-right also, which shows that despite the expected rise of the maximum electron temperature with increasing discharge voltage, the magnetic

field is highly effective in reducing the conduction of heat from the near-exit to the anode. Referring to Fig. 7-right, we note that the intersection of the grazing magnetic field line and channel centerline occurs at approximately  $z/L_c=0.15$  where  $T_e$  for all discharge voltages is approximately the same.

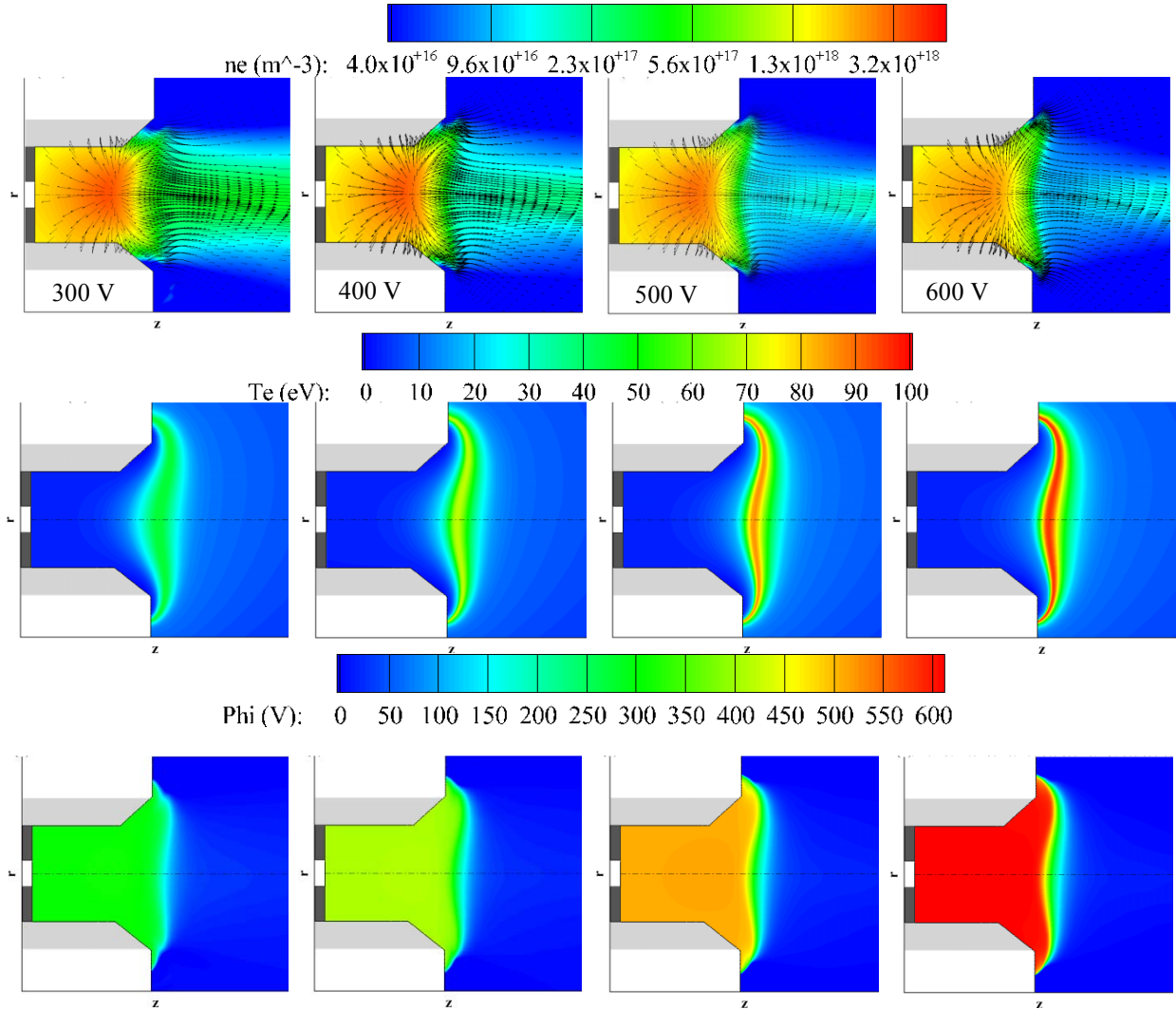


Fig. 8. Computed  $n_e$ ,  $T_e$  and  $\phi$  contours from the H6MS numerical simulations in the discharge voltage range of 300-600 V. The  $n_e$  contours are overlaid by flux vectors of singly-charged xenon ions.

The consequence is that the total energy of ions, which accounts for both the energy gained in the plasma and through the sheath, remains low as plotted in Fig. 10-left. We find for example that the maximum energy of singly-charged ions striking the inner wall is between 25-50 V for all discharge voltages. At the outer wall the maximum energy does not exceed 25 V for all discharge voltages except at 300 V and 700 V where we find values at the most downstream edge to be 30.1 V and 28 V, respectively. The erosion rate at the inner wall is found to be nearly constant with discharge voltage, and not exceeding  $10^{-2}$  mm/kh. At the outer wall the erosion rate is less than  $7.6 \times 10^{-3}$  mm/kh. These values are about three orders of magnitude lower than the maximum erosion rate measured in the unshielded H6 thruster at 300 V, as illustrated in Fig. 10-right.

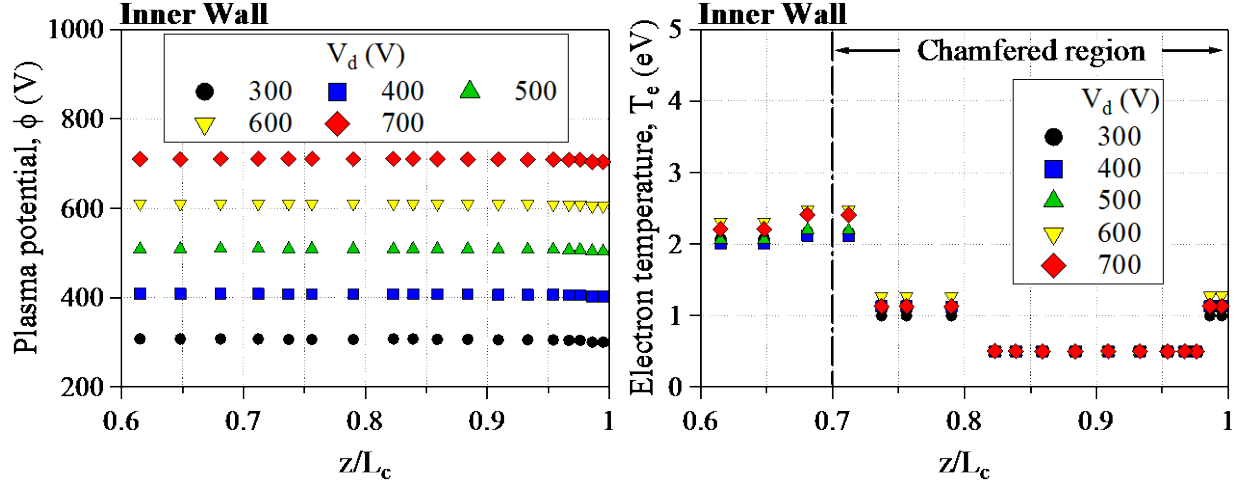


Fig. 9. Computed  $\phi$  (left) and  $T_e$  (right) along the inner channel wall of the H6MS for various discharge voltages. The potential remains fairly constant and the temperature is  $\leq 2.5$  eV, confirming that magnetic shielding remains effective for all discharge voltages. This is largely because the grazing magnetic field lines extend deep into acceleration channel where electrons remain cold despite increases in the maximum  $T_e$  with increasing discharge voltage. The results are similar at the outer wall.

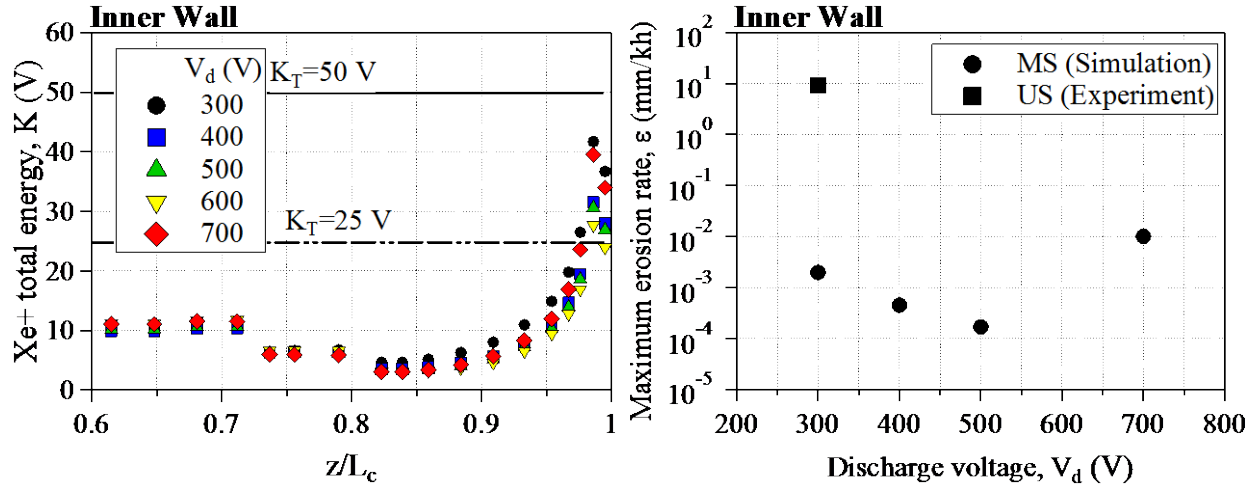


Fig. 10. Left: Total energy (plasma + sheath) of singly-charge ions along the inner wall of the H6MS at various discharge voltages. The two horizontal lines at 25 and 50 V bound the range of sputtering yield thresholds assumed for the channel material. Right: Computed maximum erosion rate at the inner wall of the H6MS for various discharge voltages. Also shown for comparison is the maximum erosion rate, averaged over several circumferential locations around the inner ring, as measured in the unshielded thruster H6US at 300 V [6].

### III. Simulation Results and Comparisons with Experiments at the 9-kW Power Level

#### A. Plasma properties

Motivated by operating conditions required for ARM, the Hall thruster was tested at 9 kW and 800 V for performance and wear in the Owens vacuum facility at JPL. Several diagnostics were employed during the tests including among others a thrust stand, current probes for measuring discharge current oscillations, thermocouples and a thermal camera, anode pressure transducer, far-field Faraday probe, and a Quartz Crystal Microbalance (QCM) and witness plates for measuring the rate of carbon deposition rate. The wear test lasted for approximately 115 h. A detailed report of the experimental campaign is planned

for the near future. In this section we present results from Hall2De simulations aimed at elucidating the expected behavior of the plasma and wall erosion at this higher power level and discharge voltage.

The numerical simulations were performed at the following operating conditions provided to us directly from the experiments (approximately 4 h into the wear test):

Table 3. Operating conditions of the H6 thruster in the 9MS800 configuration as used in the numerical simulations.

Operating Parameter	Condition
Discharge power (kW)	9.01
Discharge voltage (V)	800.1
Discharge current (A)	11.26
Anode flow rate (mg/s)	12.31
Cathode flow rate (mg/s)	0.86
Chamber pressure (Torr)	$1.2 \times 10^{-5}$

Because this (nominally) 6-kW laboratory Hall thruster was not designed to operate at the 9-kW 800-V level, magnetic circuit limitations did not allow us to achieve the most effective magnetic shielding topology in this configuration. These differences are discussed in more detail later in this section. Despite these limitations it was nevertheless possible to retain the same location of the maximum value of the magnetic field along the channel CL as that during the 6MS300 operation. The radial component of the field at the 9MS800 condition is compared to that in the 6MS300 in Fig. 11-left. Measurements of the applied magnetic field prior to the wear test were performed using a 3-axis gaussmeter that spanned the acceleration channel and the near plume region. Because in the far plume only negligible differences in the topology of the field were expected, the measurements were blended with those in the 6MS300 in the far plume and then the combined solution was implemented in Hall2De to construct the MFAM. The computed electron temperature and plasma potential along the channel centerline are compared with those for the 6MS300 condition in Fig. 11-right. We find no unexpected trends in the solution. The majority of the acceleration during the 9MS800 operation takes place between  $1 < z/L_c < 1.5$ , the region where the magnetic field at the centerline also achieves its maximum. No plasma measurements were available at the time of these simulations but, as in the results at the 6-kW level, it is likely that the maximum electron temperature,  $\sim 160$  eV (20% of  $V_d$ ), is overestimated by approximately 30%. The measured thrust ( $\sim 386$  mN after 114 h) was underestimated in the simulations by 5.9 %.

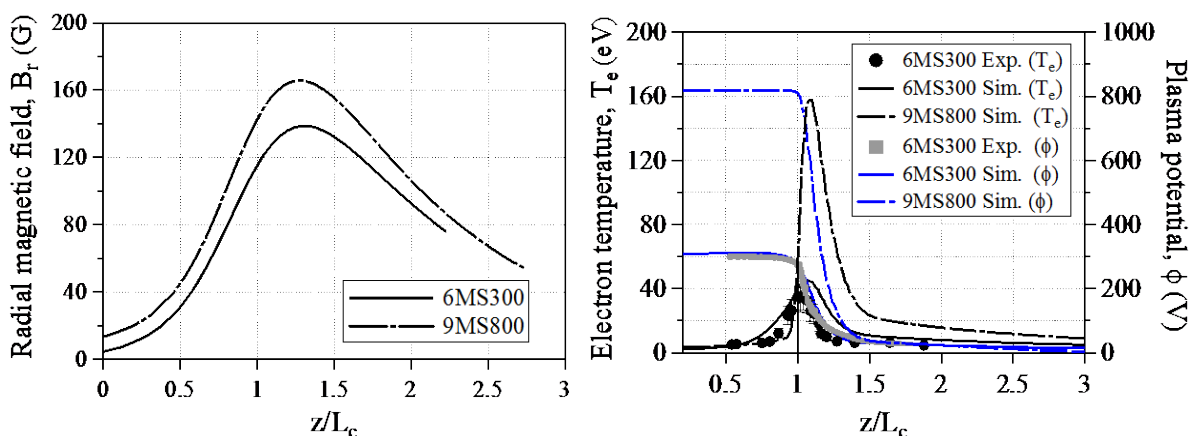


Fig. 11. Left: Comparison between  $B_r$  along the channel CL in the 6-kW MS thruster at 300 V and the 9-kW MS thruster at 800 V. Both profiles are from direct measurements using a 3-axis gaussmeter. Right: Comparison between the computed  $T_e$  and  $\phi$  along the channel centerline, for the 6MS300 and 9MS800 conditions. Also shown for reference are the plasma measurements for the 6MS300. No such measurements were available at the 9MS800 condition.

An important distinction between the 9-kW and the 6-kW operations was the magnetic field topology near the channel walls. Briefly, due to saturation of the magnetic circuit at 9 kW and 800 V it was not possible to extend the grazing magnetic field line along the inner wall as far upstream from the channel exit as that during the 6MS300 operation, as illustrated in Fig. 12 (a). More detail on the magnetic circuit limitations will be provided with our report on the experiments in a near-future publication. Thus, it was expected that due to the higher electron temperature of this grazing line of force — caused by (1) its closer proximity to the downstream region of hot electrons and (2) the higher operating discharge voltage — the erosion rates could be higher at least at the two edges closest to this line. To the contrary, magnetic shielding of the outer wall was expected to be as effective as in the 6MS300 since the location of the grazing line along this wall was not significantly different in the 9MS800, as seen by the comparison in Fig. 12 (a). Indeed, visual inspection of the insulator rings upon the conclusion of the wear test showed that, compared to the fully-darkened(grayed) surface of the during the 6MS300 operation in Fig. 12 (c) [6, 7], a light discoloration appeared around the two edges at 9MS800 inner wall (indicated by the two arrows in Fig. 12 (d)). As it was described in previous publications [6, 7], the darkening of the boron nitride channel walls, which are originally of white color, occurs due to deposition of carbon from the vacuum chamber and is an indication that erosion rates have been reduced significantly. For comparison, also shown in Fig. 12 (b) is a photograph of the inner ring at the 6US300 condition after 28 h of operation. The photograph shows a clear discoloration of the BN which is caused by the impingement of high-energy ions onto the surface. Along this “erosion band” the erosion rate greatly exceeds the carbon deposition rate. The extent of the band was measured to be  $z/L_c \sim 0.1$  which is consistent also with profilometry measurements.[6]

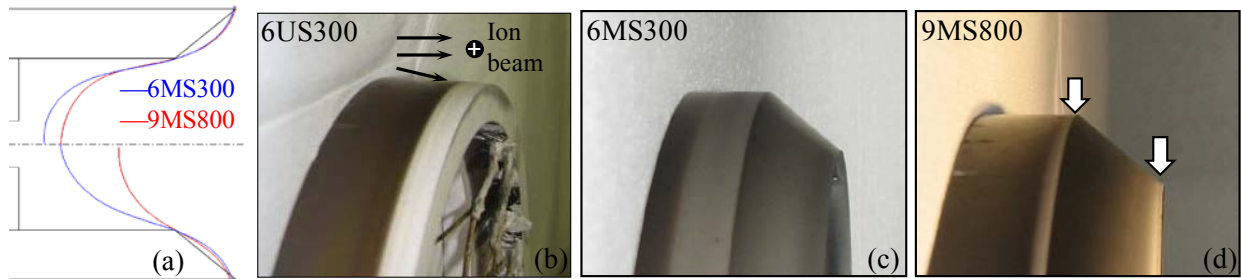


Fig. 12. (a) Comparison of grazing magnetic field lines during the 6MS300 and 9MS800 conditions. Because the Hall thruster was not designed to operate at the 9-kW, 800-V level, magnetic circuit limitations did not permit in the 9MS800 configuration the precise reproduction of the magnetic shielding topology achieved at the 6-kW power level. (b) After 28 h of operation a white-colored band was visible in the US configuration that covered the last ~10% of the channel. The extent of this band correlated very well with profilometry measurements of the erosion zone. (c) Photograph of the inner ring at the 6MS300 condition after a ~14-h wear test showing that the surface was completely covered with carbon. (d) Photograph of the inner ring in its 9MS800 configuration after a ~115-h wear test showing that carbon deposition coverage was not uniform. The two arrows point to regions/bands of lighter color than the remainder of the surface.

A closer look at the simulation results explains the observations in the wear test (Fig. 12 (d)). The computed electron temperature contours from the 9MS800 simulations are shown in Fig. 13-left. Also shown are the grazing magnetic field line along the inner wall and a line that passes by the downstream edge of the chamfered wall. Point A is at  $z/L_c = 0.46$  which is  $\Delta z/L_c = 0.26$  downstream of the intersection between the grazing line and the centerline at the 6MS300 condition. The electron temperature at points A and B is computed to be 4.3 eV. At this value we find the total energy of ions at point B to be below the minimum sputtering yield threshold of  $K_1 = 25$  V and therefore no erosion is predicted by the simulation as shown in Fig. 13-right. However, because the sputtering yield at these low energies is extremely sensitive to changes in the ion energy, a sensitivity analysis on the dependence of erosion rate on  $T_e$  reveals that a

change of only  $\sim 1.5$  eV would force the erosion rate at this point to exceed the carbon deposition rate of  $2.5 \times 10^{-3}$  mm/kh that was measured during the wear test. We find the plasma potential along the inner wall to be held very near to the discharge voltage so the increase in the erosion rate is caused largely by changes in the energy gained by ions in the sheath. Based on the Hobbs and Wesson solution [19], the sheath potential along the insulator walls is a strong function of the electron temperature and as a consequence we find that at point B an increase of 1.5 eV yields an increase of  $\sim 6$  V in the sheath potential, which is sufficient to raise the total ion energy above the assumed sputtering threshold. Similar arguments on the sensitivity of the erosion rate can be made also for the downstream edge of the chamfered region where the temperature is computed to be 5.9 eV. It is noted that changes of 1.5 eV ( $\sim 0.1$  % of the maximum  $T_e$ ) are well within both the simulation and experimental uncertainties. It is therefore argued that the discoloration at the two edges in Fig. 12 (d) was indeed caused by a higher erosion rate that was due largely to a slightly higher-than-desired  $T_e$  of the grazing line. Though unfavorable and easily fixable in a new thruster design, this feature serves as additional confirmation of our understanding of magnetic shielding physics. As expected, no such discolorations were observed at the outer wall since the location of the grazing line at the outer wall of the 9MS800 configuration was not significantly different than the one in the 6MS300. Detailed photographs of the wear-tested insulator rings and analyses of all the experimental results are planned for a future publication by Hofer *et al.*

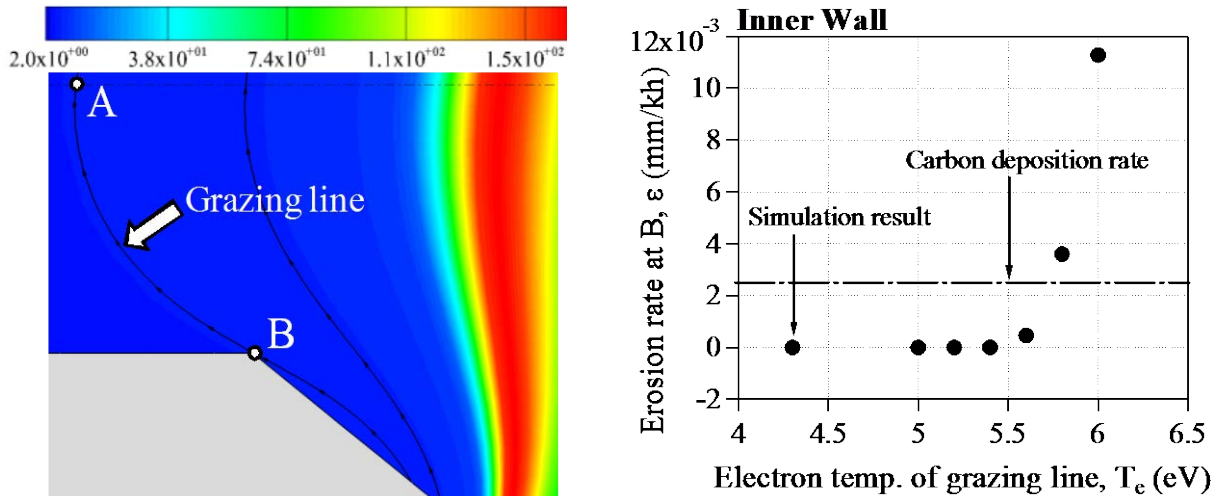


Fig. 13. Left: Computed electron temperature contours (in units of eV) in the vicinity of the inner wall from the simulations of the 9MS800 condition. Also shown is the magnetic field grazing line (passing through points A and B) and a line that just grazes the downstream edge of the chamfered wall. The electron temperature along the upstream and downstream lines is 4.3 eV and 5.9 eV, respectively. Right: Computed erosion rate at point B as a function of the electron temperature. Only  $\sim 1.5$  eV higher  $T_e$  along the A-B grazing line would force the erosion rate ( $2.5 \times 10^{-3}$  mm/kh) to exceed the measured carbon deposition rate; this value is well within the computational and experimental uncertainties.

The total kinetic energy of ions bombarding the inner and outer walls during the 9MS800 operation, as determined by the simulations, is compared in Fig. 14-left. We find that the ion energy at the outer wall is below the minimum sputtering threshold of  $K_{T1}=25$  V so no erosion is expected here. At the inner wall we find that the ion energy exceeds the 25-V threshold but is below the 50-V maximum (also depicted in Fig. 14-left as the two horizontal lines). Assuming  $K_{T1}=25$  V, Fig. 14-right plots the computed erosion rate at the inner wall. We find that the maximum of  $\sim 0.15$  mm/kh is almost two orders of magnitude less than the value measured in the unshielded thruster at 300 V. For reference, the measured carbon deposition rate was  $2.5 \times 10^{-3}$  mm/kh. As explained in previous publications (e.g. [6, 7]), it is worth noting that carbon build-up on the thruster surfaces occurs even when the erosion rate of BN exceeds the rate of carbon deposits.

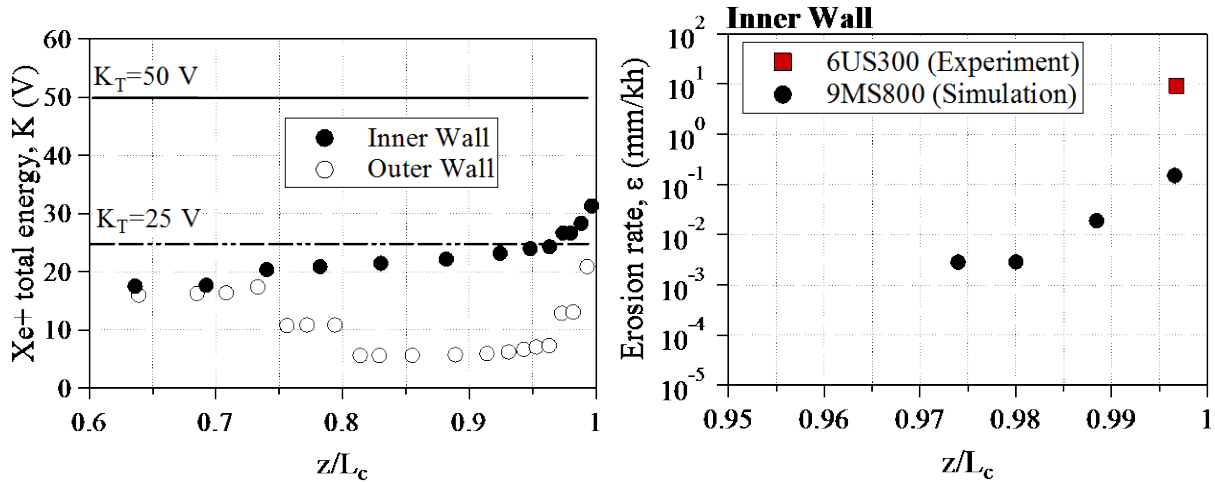


Fig. 14. Left: Computed energy of singly-charged ions striking the channel walls in the the 9MS800 configuration. The two horizontal lines at 25 and 50 V bound the range of possible sputtering yield thresholds for the channel material (BN). Right: Computed erosion rate of BN at the inner wall. Also shown is the maximum erosion rate (averaged over four circumferential locations around the ring) as measured during the (unshielded) 6US300 operation of this thruster.

#### IV. Conclusions

During a 2-yr research program that started at JPL in 2009 the first principles of magnetic shielding were derived and demonstrated for the first time in a modified (“MS”) version of the H6 Hall thruster at 6 kW and 300 V. Magnetic shielding was enabled by first, the BPT-4000, designed and built by Aerojet, that demonstrated a zero-erosion state after 5,600h of qualification testing and second, the numerical simulations and theoretical work performed at JPL that explained the physics behind these test results, including the reasons this thruster exhibited typical erosion rates in the beginning of the test.

Motivated by recent mission studies in support of ARM an effort to assess the effectiveness of magnetic shielding at discharge voltages >300 V began at JPL and NASA GRC that combined both numerical simulations and experiments. This paper has reported on the first simulation results of a magnetically shielded thruster in the range of 300-800 V. Near-future publications are planned to report on the results of the experimental campaigns.

The simulations at 6 kW and the range of 300-700 V show that, if properly designed relative to the channel geometry, the applied magnetic field can provide highly effective shielding of the walls despite the rise in the electron temperature and plasma potential expected with the increasing discharge voltage. This is because if the channel is long enough electrons near the anode can cool rapidly upon traversing the acceleration zone where most of their heating takes place. Then, if the grazing lines of force extend deep enough into the channel their temperature will remain low enough to eliminate or reduce significantly parallel gradients of the plasma potential near the walls. If this is achieved the magnitude of the discharge voltage is of no significance to erosion. In the range of 300-700 V we compute erosion rates that were ~3 orders of magnitude less than those measured in the unshielded H6 thruster at 300 V.

The importance of carefully designing the grazing lines of force has been demonstrated in additional simulations and experiments performed at 9 kW and 800 V, a condition at which this thruster was not designed to operate. As a result saturation of the magnetic circuit components did not allow us to achieve the same magnetic shielding topology as that during the 6-kW operation. Specifically, the grazing line along the inner wall appeared noticeably further downstream of its location in the H6MS. This led to a temperature in the 9MS800 configuration that, though much lower than the maximum value in the channel, was still high enough to allow for higher erosion rates near the two edges grazed by the magnetic field line at the chamfered wall. Indeed, after a ~115 h wear test of this thruster the two edges appeared

noticeably discolored compared to the rest of the chamfered region, which appeared dark due to carbon deposition. The simulations yielded a maximum erosion rate for this operating condition of 0.15 mm/kh which is ~1 order of magnitude higher than the highest value computed in the H6MS simulations but still ~2 orders of magnitude less than the value measured in the unshielded (H6US) thruster at 300 V.

### Acknowledgments

The research described in this paper was carried out by the Jet Propulsion Laboratory, California Institute of Technology, under a contract with the National Aeronautics and Space Administration and funded through the internal Research and Technology Development program. The authors wish to acknowledge Ben Jorns for providing the applied magnetic field measurements in the 9MS800 configuration of the H6 thruster.

### References

- [1] I.G. Mikellides, I. Katz, R.R. Hofer, D.M. Goebel, Magnetic shielding of walls from the unmagnetized ion beam in a Hall thruster, *Appl Phys Lett*, 102 (2013).
- [2] I.G. Mikellides, I. Katz, Numerical simulations of Hall-effect plasma accelerators on a magnetic-field-aligned mesh, *Physical Review E*, 86 (2012) 046703.
- [3] K.H. De Grys, A. Mathers, B. Welander, V. Khayms, AIAA Paper No. 10-6698, in: *Proceedings of the 46th AIAA/ASME/SAE/ASEE Joint Propulsion Conference*, Nashville, TN, 2010, pp. 6698.
- [4] I.G. Mikellides, I. Katz, R.R. Hofer, D.M. Goebel, K. de Grys, A. Mathers, Magnetic shielding of the channel walls in a Hall plasma accelerator, *Physics of Plasmas*, 18 (2011) 033501.
- [5] I.G. Mikellides, I. Katz, R.R. Hofer, AIAA Paper No. 11-5809, in: *Proceedings of the 47th AIAA Joint Propulsion Conference*, San Diego, CA, American Institute of Aeronautics and Astronautics, Washington, DC, 2011, pp. 5809.
- [6] R.R. Hofer, D.M. Goebel, I.G. Mikellides, I. Katz, AIAA Paper No. 12-3788, in: *Proceedings of the 48th AIAA Joint Propulsion Conference*, Atlanta, GA, American Institute of Aeronautics and Astronautics, Washington, DC, 2012, pp. 3788.
- [7] I.G. Mikellides, I. Katz, R.R. Hofer, D.M. Goebel, AIAA Paper No. 12-3789, in: *Proceedings of the 48th AIAA Joint Propulsion Conference*, Atlanta, GA, American Institute of Aeronautics and Astronautics, Washington, DC, 2012, pp. 3789.
- [8] J.M. Haas, R.R. Hofer, D.L. Brown, B.M. Reid, A.D. Gallimore, in: *54th JANNAF Propulsion Meeting*, Johns Hopkins University, Chemical Propulsion Information Analysis Center (CPIAC), Denver, CO, 2007.
- [9] J.R. Brophy, L. Friedman, Returning an Entire Near-Earth Asteroid in Support of Human Exploration Beyond Low-Earth Orbit, in: *IAF Global Exploration Conference*, Jet Propulsion Laboratory, National Aeronautics and Space Administration, Washington, D. C., 2012.
- [10] J.R. Brophy, L. Friedman, F. Culick, Asteroid Retrieval Feasibility, in: *Aerospace Conference*, 2012, Institute of Electrical and Electronics Engineers, Big Sky, MT, 2012, pp. 1 - 16.
- [11] J.R. Brophy, S. Oleson, AIAA Paper No. 12-4067, in: *Proceedings of the 48th AIAA Joint Propulsion Conference*, Atlanta, GA, American Institute of Aeronautics and Astronautics, Washington, DC, 2012, pp. 4067.
- [12] A.I. Morozov, Focussing of Cold Quasineutral Beams in Electromagnetic Fields, *Dokl Akad Nauk Sssr+*, 163 (1965) 1363-&.
- [13] A.I. Morozov, V.V. Savelyev, Fundamentals of Stationary Plasma Thruster Theory *Reviews of Plasma Physics*, in: B.B. Kadomtsev, V.D. Shafranov (Eds.), Springer US, 2000, pp. 203-391.
- [14] I. Katz, I.G. Mikellides, Neutral gas free molecular flow algorithm including ionization and walls for use in plasma simulations, *J Comput Phys*, 230 (2011) 1454-1464.
- [15] N.B. Meezan, W.A. Hargus, M.A. Cappelli, Anomalous electron mobility in a coaxial Hall discharge plasma, *Physical Review E*, 63 (2001).

- [16] A. Ducrocq, J.C. Adam, A. Heron, G. Laval, High-frequency electron drift instability in the cross-field configuration of Hall thrusters, *Physics of Plasmas*, 13 (2006).
- [17] A. Lazurenko, T.D. de Wit, C. Cavoit, V. Krasnoselskikh, A. Bouchoule, M. Dudeck, Determination of the electron anomalous mobility through measurements of turbulent magnetic field in Hall thrusters, *Physics of Plasmas*, 14 (2007).
- [18] C. Boniface, L. Garrigues, G.J.M. Hagelaar, J.P. Boeuf, D. Gawron, S. Mazouffre, Anomalous cross field electron transport in a Hall effect thruster, *Appl Phys Lett*, 89 (2006).
- [19] G.D. Hobbs, J.A. Wesson, Heat Flow through a Langmuir Sheath in Presence of Electron Emission, *Plasma Physics*, 9 (1967) 85-87.
- [20] R.R. Hofer, I.G. Mikellides, I. Katz, D.M. Goebel, AIAA Paper No. 07-5267, in: *Proceedings of the 43rd AIAA Joint Propulsion Conference*, Cincinnati, OH, American Institute of Aeronautics and Astronautics, Washington, DC, 2007, pp. 5267.
- [21] Y. Garnier, V. Viel, J.F. Roussel, J. Bernard, Low-energy xenon ion sputtering of ceramics investigated for stationary plasma thrusters, *J Vac Sci Technol A*, 17 (1999) 3246-3254.
- [22] A.P. Yalin, J.D. Williams, V. Surla, K.A. Zoerb, Differential sputter yield profiles of molybdenum due to bombardment by low energy xenon ions at normal and oblique incidence, *J Phys D Appl Phys*, 40 (2007) 3194-3202.
- [23] B. Rubin, J.L. Topper, A.P. Yalin, Total and differential sputter yields of boron nitride measured by quartz crystal microbalance, *J Phys D Appl Phys*, 42 (2009).
- [24] R. Shastry, *Experimental Characterization of the Near-Wall Region in Hall Thrusters and its Implications on Performance and Lifetime*, in, 2011.